Dynamical systems model of entrainment due to coherent structures

Srevatsan Muralidharan,[1,2] K. R. Sreenivas,[1] and Rama Govindarajan[1,*]
[1]*Engineering Mechanics Unit, Jawaharlal Nehru Centre for Advanced Scientific Research, Jakkur, Bangalore 560064, India*
[2]*Department of Mechanical Engineering, Indian Institute of Technology Madras, Chennai 600036, India*
(Received 13 June 2005; published 12 October 2005)

The lifetime of a turbulent shear flow is inversely related to the amount of surrounding fluid it entrains. A dynamical systems model of such a flow, dominated by coherent structures, was recently proposed [R. Govindarajan, Phys. Rev. Lett. **88**, 134503 (2002)], where an axisymmetric heated jet was modelled by a pair of leap-frogging vortex rings. In the present paper we study the equivalent two-dimensional flow, namely, two pairs of corotating point vortices, of opposite sign. We prove that the system is nonintegrable for any finite separation between the pairs, and show that entrainment is a natural consequence of chaotic advection. The effect of core diffusion due to viscosity is studied, and it is shown that the entrainment rate is reduced with increasing viscosity, by a reduction in leap-frogging frequency.

DOI: 10.1103/PhysRevE.72.046308 PACS number(s): 47.27.Nz, 47.32.Cc, 47.52.+j

I. INTRODUCTION

The flow of a jet into a surrounding quiescent fluid medium is ubiquitous, e.g., water flowing out of a faucet, or hot gasses spewing out of volcanoes. Being usually turbulent, a jet provides a good theoretical and experimental case study of a free-shear flow. Depending on the geometry of the source, a jet could be either axisymmetric, or practically planar. Probably the most significant phenonemenon taking place in a jet is that as it progresses downstream, more and more of surrounding (ambient) fluid is engulfed (in the terminology of Ref. [2]) and begins to travel with it. The new fluid then mixes with the fluid carried from the source. This process is known as entrainment. The jet thus advects an increasing mass of fluid and becomes progressively more dilute in the original fluid. Coherent vortical structures dominate such a flow. They account for a considerable fraction of the kinetic energy and play a key role in the process of entrainment.

In the vicinity of coherent structures, transport through advection is often chaotic [3]. A study of chaotic advection can give quantitative information on the engulfment and stretching of portions of fluid. A special feature of chaotic advection in vortical flows is that even when the basic flow is periodic the Lagrangian dynamics of fluid particles can be chaotic [4]. An understanding of this process could be crucial in determining how pollutant is dispersed in the atmosphere, how dangerous the trailing vortex system of a landing aircraft can be to a follower aircraft, how clouds can retain water vapor as they rise through the atmosphere, to quote but a few examples.

In two-dimensional flows, due to repeated vortex merging, isolated concentrated vortex patches are often found to form even in initially randomly distributed flows. Since the dissipation time scales of these patches are much larger than the eddy turnover times, such vortices are able to sustain themselves for long times, and a point-vortex model is often a good approximation [5].

Our purpose here is to study model vortical flows under the dynamical systems framework to quantify entrainment and the resulting chaos. In a recent paper [1], it was shown that a small level of buoyancy, which in real life would be achieved by off-source volumetric heating of the flow relative to the surroundings, can modify the entrainment drastically, and on occasion even shut it off completely. The predictions made in the paper were found to be in qualitative agreement with those made by direct numerical simulations [6] and experiments [7]. In the present paper, for better understanding of the physics involved, we consider the two-dimensional analog of the flow considered in Ref. [1], namely, two pairs of point vortices. In the inviscid limit, these vortex pairs perform a periodic leap-frogging motion, as follows. For the instant of time shown in Fig. 1, the pair of counter-rotating vortices at $x=x_1$ move with greater speed than the pair at $x=x_2$. The separation between the vortices at the rear decreases until they overtake the pair in front, and increases thereafter. The process is repeated with a frequency dependent on the initial streamwise separation. The four vor-

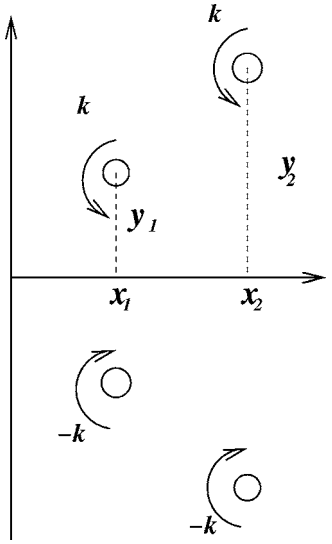

FIG. 1. Configuration of the leap-frogging vortex pairs.

*Electronic address: rama@jncasr.ac.in

tices here will be referred to as LFVP, for leap-frogging vortex pairs. The Lagrangian fluid motion due to LFVP was numerically studied by Pentek *et al.* [4]. The system was found to be strongly nonlinear and the presence of hyperbolic fixed points was found responsible for the chaotic nature of the flow. It can easily be demonstrated that transport and entrainment of the ambient fluid into the flow are natural consequences of the tangling of the manifolds arising from the hyperbolic fixed points of this system. The flow dynamics is area and orientation preserving [8], these and other properties of the manifolds are exploited here to obtain the entrainment quantitatively, and estimate chaos and mixing.

The two main results of this paper are as follows: (i) the motion of the surrounding fluid due to LFVP is proved nonintegrable for any finite separation between the vortex pairs. (ii) Viscosity is shown to have a mitigating influence on the leap-frogging behavior, and hence on the entrainment.

The rest of the paper is organized as follows. The basic equations are written in Sec. II. The nonintegrability of the flow is discussed in Sec. III, Sec. IV discusses the effect of buoyancy on entrainment, and Sec. V is devoted to the effect of viscosity.

II. INVISCID FLOW: BASIC EQUATIONS

The governing equations that describe the motion of the LFVP are Hamiltonian, and since the flow is symmetric with respect to the x axis, the Hamiltonian for the symmetry-reduced problem can be written as follows [4]:

$$H(x_i,y_i)=\frac{k^2}{2\pi}\ln\left(4y_1y_2\frac{(x_1-x_2)^2+(y_1+y_2)^2}{(x_1-x_2)^2+(y_1-y_2)^2}\right)=E \quad (1)$$

and

$$k_i\dot{x}_i=\frac{\partial H}{\partial y_i},\quad k_i\dot{y}_i=-\frac{\partial H}{\partial x_i}. \quad (2)$$

The energy E and the average distance $(y_1+y_2)/2$ of the vortices from the x axis are integrals of the motion. For $E>0$, the motion of the vortices themselves, as discussed above, is that of a periodic leap frog [4]. The Lagrangian motion of a fluid particle due to the presence of these vortices, however, is much more complicated. The latter is described by the streamfunction

$$\Psi(x,y,t)=-\Sigma_j\frac{k_j}{\pi}\ln r_j(t), \quad (3)$$

where

$$v_x(x,y,t)=\frac{\partial\Psi}{\partial y}\quad\text{and}\quad v_y(x,y,t)=-\frac{\partial\Psi}{\partial x} \quad (4)$$

are the streamwise and normal components of velocity, respectively.

III. NONINTEGRABILITY OF FLOW DUE TO THE LFVP

We prove analytically here that the tracer particle dynamics is nonintegrable. Bagrets *et al.* [9] addressed the problem of nonintegrability of more than two vortex rings using the method of splitting of separatrices (more commonly known as the Melnikov technique). We use the same principle to prove the nonintegrability of our system.

In what follows, we first consider a single corotating vortex pair, for example, the pair lying below the x axis in Fig. 1. In the absence of any other vorticity, this pair executes motion on a circle, and the flow induced in the surroundings is integrable. This will be our zeroth-order solution. A second pair is then introduced at a very large (vertical, in the figure) distance, from the first pair, such that the influence of the newly introduced pair on the flow in the vicinity of the original pair may be treated as a perturbation on the original flow. The first order term in the resulting perturbation expansion is shown to have no influence except on the mean velocity. The second-order term ensures that the system is nonintegrable for any finite vertical separation. Using this, we demonstrate that the process of entrainment is a natural consequence of the chaotic nature of the advection.

The motion of all four point vortices is described by

$$\frac{2\pi}{k}\frac{dx_i}{dt}=\frac{1}{y_i}+\frac{2(y_i+y_j)}{(x_i-x_j)^2+(y_i+y_j)^2}-\frac{2(y_i-y_j)}{(x_i-x_j)^2+(y_i-y_j)^2}, \quad (5)$$

$$\frac{2\pi}{k}\frac{dy_i}{dt}=\frac{2(x_i-x_j)}{(x_i-x_j)^2+(y_i+y_j)^2}-\frac{2(x_i-x_j)}{(x_i-x_j)^2+(y_i-y_j)^2}, \quad (6)$$

where the index $i=1,2$ (see Fig. 1) and $j=2$ when $i=1$ and vice versa. Without loss of generality we may take $k=\pi$. We then make the transformation [9], $x_i\to\epsilon\tilde{x}_i$, $y_i\to 1+\epsilon\tilde{y}_i$, $t\to\epsilon^2\tilde{t}$, where $i=1,2$; and define $\tilde{x}_r\equiv\tilde{x}_1-\tilde{x}_2$, and $\tilde{y}_r\equiv\tilde{y}_1-\tilde{y}_2$. The small parameter ϵ is of $O(x_r/y_r)$.

In the new variables Eqs. (5) and (6) reduce to

$$\frac{d\tilde{x}_r}{d\tilde{t}}=-\frac{2\tilde{y}_r}{\tilde{x}_r^2+\tilde{y}_r^2}-\epsilon^2\frac{\tilde{y}_r}{2}+o(\epsilon^3), \quad (7)$$

$$\frac{d\tilde{y}_r}{d\tilde{t}}=\frac{2\tilde{x}_r}{\tilde{x}_r^2+\tilde{y}_r^2}-\epsilon^2\frac{\tilde{x}_r}{2}+o(\epsilon^3). \quad (8)$$

Equation (7) and (8) have a solution of the form

$$\begin{bmatrix}\tilde{x}_r\\ \tilde{y}_r\end{bmatrix}=\begin{bmatrix}\tilde{x}_{r0}+\epsilon^2\tilde{x}_{r2}+o(\epsilon^3)\\ \tilde{y}_{r0}+\epsilon^2\tilde{y}_{r2}+o(\epsilon^3)\end{bmatrix}. \quad (9)$$

The zeroth-order solution is given by $\tilde{x}_{r0}=2\cos(\tilde{t}/2)$ and $\tilde{y}_{r0}=2\sin(\tilde{t}/2)$, which represents motion on the circumference of a circle, and the second-order term satisfies

$$\frac{d}{d\tilde{t}}\begin{bmatrix}\tilde{x}_{r2}\\ \tilde{y}_{r2}\end{bmatrix}=\begin{bmatrix}(\sin\tilde{t})/2 & -(\cos\tilde{t})/2\\ -(\cos\tilde{t})/2 & -(\sin\tilde{t})/2\end{bmatrix}\begin{bmatrix}\tilde{x}_{r2}\\ \tilde{y}_{r2}\end{bmatrix}-\begin{bmatrix}\sin(\tilde{t}/2)\\ \cos(\tilde{t}/2)\end{bmatrix}. \quad (10)$$

The solution is

$$\tilde{x}_{r2}=\sin(\tilde{t})\sin(\tilde{t}/2)-\tilde{t}\sin(\tilde{t}/2)+\lambda_1[\tilde{t}\sin(\tilde{t}/2)+\cos(\tilde{t}/2)]-\lambda_2\sin(\tilde{t}/2), \quad (11)$$

$$\tilde{y}_{r2} = -\sin(\tilde{t})\cos(\tilde{t}/2) + \tilde{t}\cos(\tilde{t}/2) - 2\sin(\tilde{t}/2) + \lambda_1 \sin(\tilde{t}/2) - \lambda_1 \tilde{t}\cos(\tilde{t}/2) + \lambda_2 \cos(\tilde{t}/2). \quad (12)$$

λ_1 and λ_2 are the second-order corrections at $t=0$ to x_r and y_r, respectively.

The terms whose amplitudes are linear in time may be recognized as secular terms [10], which often arise due to improper treatment of the system's frequency. In other words, the frequency of the perturbed system is no longer $1/2$, but has an $O(\epsilon^2)$ correction. Accounting for this, one obtains

$$\tilde{x}_r = 2\cos\omega\tilde{t} + \epsilon^2[\sin(\tilde{t})\sin(\tilde{t}/2) + \lambda_1\cos(\tilde{t}/2) - \lambda_2\sin(\tilde{t}/2)] + o(\epsilon^3), \quad (13)$$

$$\tilde{y}_r = 2\sin\omega\tilde{t} + \epsilon^2[-\sin(\tilde{t})\cos(\tilde{t}/2) - 2\sin(\tilde{t}/2) + \lambda_1\sin(\tilde{t}/2) + \lambda_2\cos(\tilde{t}/2)] + o(\epsilon^3), \quad (14)$$

where

$$\omega = \omega_0 + \epsilon^2\Delta\omega, \quad (15)$$

with $\omega_0 = 1/2$ and $\Delta\omega = (1-\lambda_1)/2$.

On performing the stretching transformation, $x \to \epsilon\tilde{x}$ and $y \to \epsilon\tilde{y}$, Eqs. (4), describing the motion of a tracer particle in the vicinity can be reduced to

$$\frac{d\tilde{x}}{d\tilde{t}} = -\left(\frac{\tilde{y}-\tilde{y}_1}{(\tilde{x}-\tilde{x}_1)^2+(\tilde{y}-\tilde{y}_1)^2} + \frac{\tilde{y}-\tilde{y}_2}{(\tilde{x}-\tilde{x}_2)^2+(\tilde{y}-\tilde{y}_2)^2}\right) + \epsilon - \epsilon^2\frac{\tilde{y}}{2} + o(\epsilon^3), \quad (16)$$

$$\frac{d\tilde{y}}{d\tilde{t}} = \left(\frac{\tilde{x}-\tilde{x}_1}{(\tilde{x}-\tilde{x}_1)^2+(\tilde{y}-\tilde{y}_1)^2} + \frac{\tilde{x}-\tilde{x}_2}{(\tilde{x}-\tilde{x}_2)^2+(\tilde{y}-\tilde{y}_2)^2}\right) - \epsilon^2\frac{\tilde{x}}{2} + o(\epsilon^3). \quad (17)$$

Since,

$$\frac{1}{2}\left(\frac{d\tilde{x}_1}{d\tilde{t}} + \frac{d\tilde{x}_2}{d\tilde{t}}\right) = \epsilon + o(\epsilon^3), \quad (18)$$

in a coordinate system traveling with the midpoint of the line joining the first corotating pair, one obtains the following streamfunction for the Lagrangian particle:

$$\Psi = -\frac{1}{2}\ln\{[(\tilde{x}-\tilde{x}_1)^2+(\tilde{y}-\tilde{y}_1)^2][(\tilde{x}-\tilde{x}_2)^2+(\tilde{y}-\tilde{y}_2)^2]\} + \frac{\epsilon^2}{4}(\tilde{x}^2-\tilde{y}^2) + o(\epsilon^3). \quad (19)$$

The variables now denote position in the moving coordinate system. To simplify the algebra we define $\tilde{z}=\tilde{x}+i\tilde{y}$, $\tilde{z}_1 = e^{i\omega t} + \epsilon^2/2\tilde{z}_{r2}$, where $\tilde{z}_{r2}=\tilde{x}_{r2}+i\tilde{y}_{r2}$. Due to the choice of the coordinate system, $\tilde{z}_2 = -\tilde{z}_1$. Equation (19) now reads as

$$\Psi = -\ln|\tilde{z} - (e^{i\omega t} + \epsilon^2\tilde{z}_{r2})| - \ln|\tilde{z} + (e^{i\omega t} + \epsilon^2\tilde{z}_{r2})| + \frac{\epsilon^2}{8}(\tilde{z}^2 + \bar{\tilde{z}}^2) + o(\epsilon^3), \quad (20)$$

which on performing a rotation transform $\tilde{z} \to \tilde{z}e^{i\omega t}$ reduces to

$$\Psi = -\ln|\tilde{z}-1| - \ln|\tilde{z}+1| + \epsilon^2\left[\mathrm{Re}\left(\frac{\tilde{z}_{r2}e^{-i\omega_0 t}}{\tilde{z}-1}\right) - \mathrm{Re}\left(\frac{\tilde{z}_{r2}e^{-i\omega_0 t}}{\tilde{z}+1}\right) + \frac{1}{8}(\tilde{z}^2e^{2i\omega_0 t} + \bar{\tilde{z}}^2e^{-2i\omega_0 t})\right] + \frac{1}{2}\omega|\tilde{z}|^2 + o(\epsilon^3). \quad (21)$$

It is to be noted that the last term in the above expression arises due to the rotation transformation. The final streamfunction one obtains after resubstituting z as $x+iy$ is of the form $\Psi_0 + \epsilon^2\Psi_2 + o(\epsilon^3)$, where

$$\Psi_0 = -\tfrac{1}{2}\{\ln[(\tilde{x}-1)^2+\tilde{y}^2] + \ln[(\tilde{x}+1)^2+\tilde{y}^2]\} + \tfrac{1}{4}(\tilde{x}^2+\tilde{y}^2) \quad (22)$$

and

$$\Psi_2 = \{[\lambda_1 - 2\sin^2(\tilde{t}/2)](\tilde{x}-1) + [\lambda_2 - 2\sin(\tilde{t})]\tilde{y}\}/\{2[(\tilde{x}-1)^2+\tilde{y}^2]\} - \{[\lambda_1 - 2\sin^2(\tilde{t}/2)](\tilde{x}+1) + [\lambda_2 - 2\sin(\tilde{t})]\tilde{y}\}/\{2[(\tilde{x}+1)^2+\tilde{y}^2]\} + \tfrac{1}{4}\{(\tilde{x}^2-\tilde{y}^2)\cos(\tilde{t}) - 2\tilde{x}\tilde{y}\sin(\tilde{t})\} + \tfrac{1}{4}(1-\lambda_1)(\tilde{x}^2+\tilde{y}^2). \quad (23)$$

The above streamfunction is the same as that of Ref. [9] at zeroth order, but the higher orders differ. The zeroth-order manifold describing the motion due to a single pair of corotating vortices resembles the structures obtained by Ref. [11] in the near-vortex region. The phase plot of the motion of the particles is shown in Fig. 2. The positions of the vortices are denoted by circles. The fixed points of the system are $(\pm\sqrt{5},0)$, (0, 0), and $(0,\pm\sqrt{3})$. The fixed point $(-\sqrt{5},0)$ has two hetroclinic orbits, $P_1O_1P_2P_1$ and $P_1O_2P_2P_1$, and the fixed point (0, 0) has a homoclinic orbit as shown in Fig. 2. The stable and unstable manifolds of the unperturbed Hamiltonian (Ψ_0) are coincident. More important, these manifolds are streamlines and act as total barriers to fluid transport. It is when these manifolds are no longer coincident that entrainment can take place, we shall see below that entrainment and chaos are therefore directly connected.

On perturbing this flow by Ψ_2 as in Eq. (21), the stable and unstable manifolds split. Any transverse intersection of these manifolds guarantees the nonintegrability of the system [13]. The check for transverse intersection may be done by evaluating the Melnikov function, defined by [8,13]

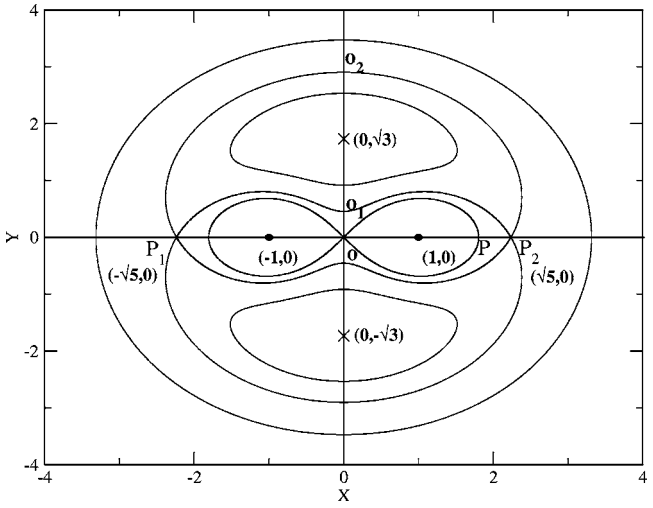

FIG. 2. The manifolds of the hetroclinic and homoclinic fixed points of the unperturbed Hamiltonian. The vortices are located at $(-1,0)$ and $(1,0)$. P_1, O, and P_2 are hyperbolic fixed points, while $(0,\pm\sqrt{3})$ are elliptic fixed points.

$$M(t_0) \equiv \int_{-\infty}^{\infty} \{\Psi_0, \Psi_2\}(x(t), y(t), t + t_0)dt, \tag{24}$$

where $\{,\}$ is the Poisson bracket and t_0 parametrizes the unperturbed manifold.

The distance between the stable and the unstable manifolds is directly proportional to the Melnikov function, and is given by

$$d(\epsilon^2, t_0) = -\epsilon^2 \frac{M(\epsilon^2, t_0)}{\Psi_0(x(t_0), y(t_0))}. \tag{25}$$

Hence, the manifolds intersect everytime $M(t_*)=0$ for some $t_*=t_0$. Further, if $\partial M/\partial t_* \neq 0$ (which defines a simple zero at t_*) then the manifolds intersect transversely [8]. A numerical integration of Eq. (24) using Eqs. (22) and (23) is performed for sufficiently large times over the unperturbed manifold, and as $t \to \pm\infty$ the trajectories of particles approach the stable and unstable fixed points. The integration was performed for three manifolds, namely, $P_1O_1P_2$, $P_1O_2P_2$, and POP in Fig. 2. It was found that for all three manifolds that contributions from terms having coefficients λ_1, λ_2 on integration were negligible. The Melnikov functions in the three cases were found to be

$$-3.3845\cos(t_0) - 1.354\,14\sin(t_0) \quad \text{for } P_1O_1P_2,$$

$$-0.2308\cos(t_0) - 0.3857\sin(t_0) \quad \text{for } P_1O_2P_2,$$

$$\text{and } 0.2923\cos(t_0) + 0.022\,85\sin(t_0) \quad \text{for } POP.$$

It is clear that the above expressions all possess simple zeros, thus completing the proof of nonintegrability.

The splitting of the manifolds and their repeated intersection ensures the chaotic nature of the transport process. A Poincaré section, sampled once during each time period of the perturbed manifold, is plotted for increasing ϵ in Figs. 3 and 4 to show the nature of the onset of chaos in the system.

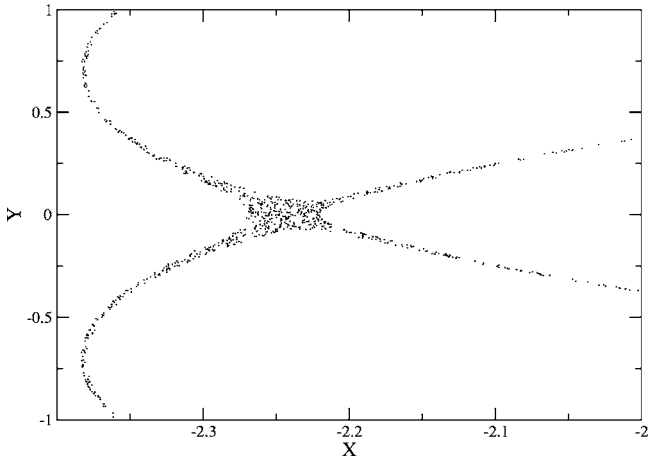

FIG. 3. The onset of chaos near the hyperbolic fixed point is shown at $\epsilon=0.01$.

On comparing with Fig. 2 one finds that trajectories which were initially constrained to move along the streamlines now sample a larger portion of the domain. Moreover, the interchange of external and internal fluid is now permissible, hence chaotic advection is seen to be a natural reason for transport. The exponential separation of the trajectories in the region close to the transverse tangling aids in the process of stretching. As $t \to \pm\infty$, since the trajectories along the separatrix approach the fixed points, the denominator of Eq. (25) tends to zero. Hence, the distance between the stable and unstable manifolds approaches infinity indicative of very large stretching near the hyperbolic fixed points. This stretching, and how chaos and entrainment are directly related, become evident in the following section where we discuss the complete inviscid problem.

IV. THE COMPLETE INVISCID PROBLEM

In the proof of nonintegrability above, we had considered the second pair of corotating vortices to be very far from the

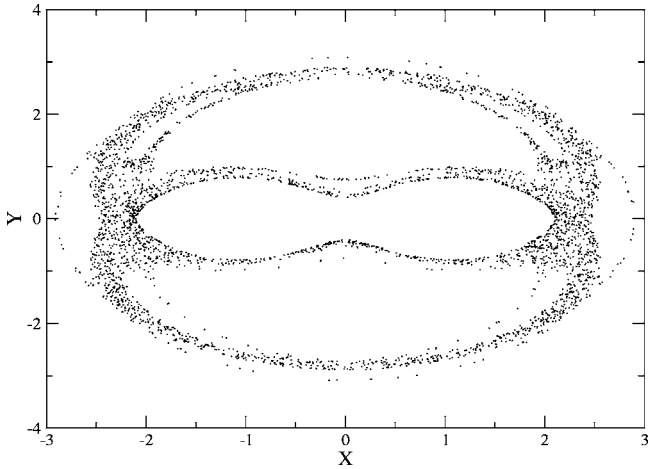

FIG. 4. Poincaré section illustrating the chaotic behavior at $\epsilon=0.1$. Chaotic advection is primarily responsible for the transport process, as the particles would otherwise be restricted to their streamlines in the unperturbed flow.

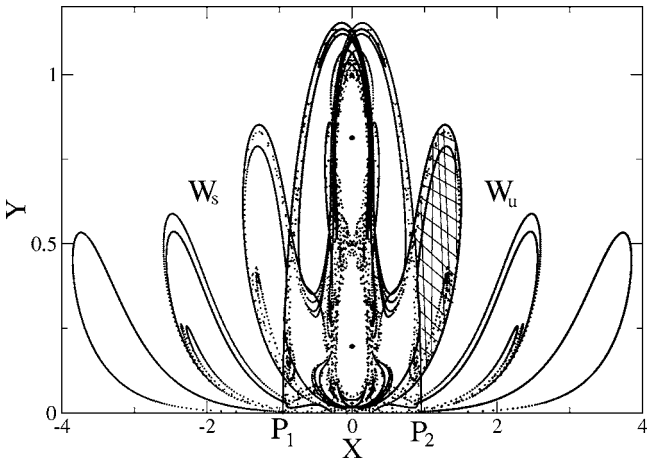

FIG. 5. A Poincaré section of the stable and unstable manifolds emerging from saddle points P_1 and P_2, respectively, depicted. If the manifolds intersect each other once, it is guaranteed that they shall intersect infinitely many times, which gives rise to the stretching behavior of the lobes shown in this figure. The area of each lobe is the same as all the others [8]. The vortices are denoted by squares.

first pair. We now consider the physics of the complete problem, for any separation between the two pairs, i.e., we solve Eqs. (1)–(4) without any approximation. A coordinate system moving with the average velocity of the vortices is chosen here to simplify the analysis. In the new coordinate system (see Fig. 1), two saddle points P_1 and P_2 are located at $y=0$. From P_2, an unstable manifold W_u emerges in the normal direction, while a stable manifold W_s approaches P_1 as shown in Fig. 5. The transverse tangling of these manifolds is evident. The manifolds and the fixed points for the complete problem, as expected, are different from those obtained in the special limit of the preceding section. Note the shift in focus from the vicinity of the corotating pair in earlier figures to the entire system here. The x axis now is the symmetry plane of the four-vortex system. In Fig. 2, the symmetry plane is located at a large negative value of y, and the fixed points P_1 and P_2 are therefore not seen. Also, note that the

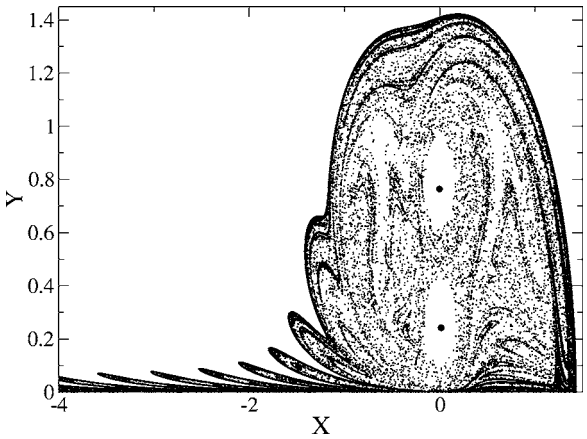

FIG. 6. The manifold of the fixed points at $u_b=-0.15$ is plotted. The lobe is seen to have negligible area and hence entrainment due to transport process is little.

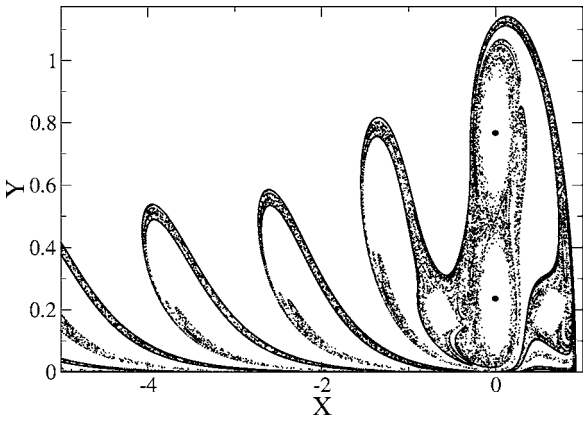

FIG. 7. Entrainment at a positive buoyancy, $u_b=0.151$, is greater than that in Fig. 6.

phase chosen for the Poincaré section in Fig. 5 is different from that of the earlier figures.

By definition, a fluid particle located on a manifold stays on it throughout its evolution in time. This immediately implies that the occurrence of one intersection of these manifolds ensures their repeated intersection infinitely many times. These transverse intersections lead to the formation of Smale-horseshoes, giving rise to chaotic flow in the neighborhood. The area of the lobes, shown as the shaded region in Fig. 5, is preserved with time evolution. Since, the orientation of each lobe with respect to the manifold remains the same, the topology of the flow is preserved, resulting in the entrainment of fluid from the external region to the internal and vice versa. These properties, and the fact that a manifold cannot intersect itself, lead to complicated stretching as shown in Fig. 5. A close look at the Fig. 5 also reveals the presence of Kolmogorov-Arnold-Moser (KAM) tori around each of the vortices. These are closed curves in the Poincaré section, serving as complete barriers to flow, and therefore play an important role in deciding entrainment and mixing. The region of interest, into and out of which entrainment is measured, is taken to be that bounded by the curves P_1O, OP_2, and P_1P_2. A detailed review of the properties of manifolds can be found in Wiggins [12]. The Poincaré section is

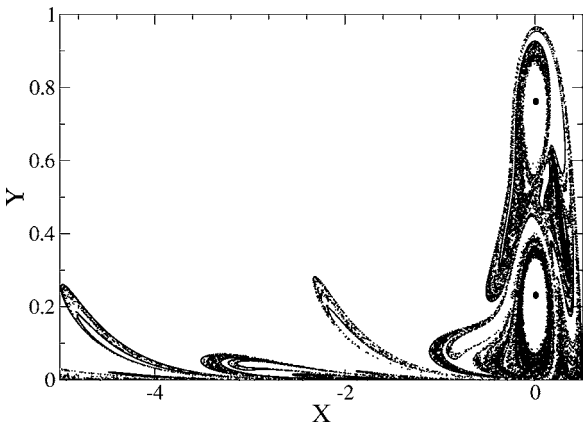

FIG. 8. At an even higher buoyancy value of $u_b=0.3$ entrainment is once again seen to decrease implying the nonmonotonous variation of entrainment with buoyancy.

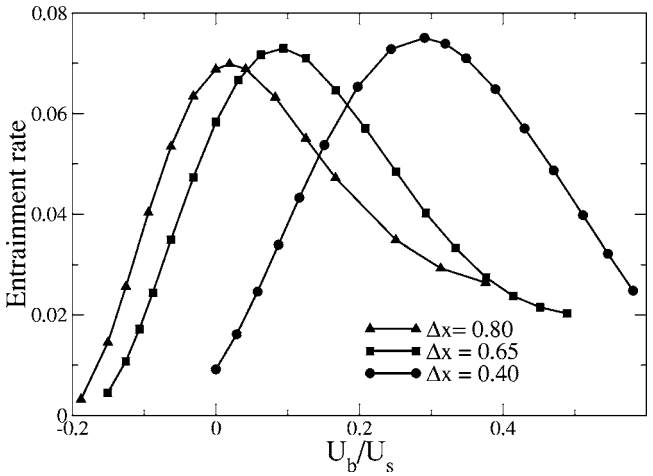

FIG. 9. The entrainment rate as a function of the buoyancy velocity. For each pair spacing, a maximum in the entrainment occurs at an optimum buoyancy velocity. The maximum in the entrainment rate is independent of pair spacing.

taken here at the phase where the vortices are aligned at $x=0$, but the results do not depend on this choice.

Effect of buoyancy: The heating or cooling of portions of a flow results in buoyancy playing a lead role in chaotic advection [1]. In particular, if the vortices are hotter or colder than the surrounding flow, the entrainment is drastically affected. This situation is modelled simply by giving the vortices an additional (buoyancy) velocity U_b of the appropriate sign. U_b results from the integrated effect of heating/cooling over a time interval [1]. An immediate effect of buoyancy on the flow topology can be seen in the change in the distance between the fixed points. For $U_b>0$ and increasing, the fixed points move closer to each other, and vanish above a critical U_b, thus shutting off the entrainment. For $U_b<0$ and decreasing, the fixed points move further apart and their separation goes to infinity below another critical U_b, again leading to a reduction in the entrainment. This implies that

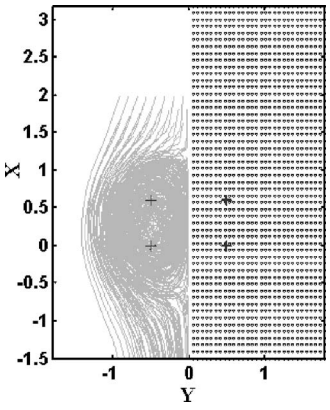

FIG. 10. The computational system. The initial positions of the vortex blobs are indicated by plus marks, with arrows showing the sense of circulation. The absolute value of the circulation is 1. The dots on the right-hand panel show the initial locations of tracer particles in half the domain. The particles are symmetrically placed on the other side as well. The trajectories of a few of the tracer particles are shown on the left-hand panel.

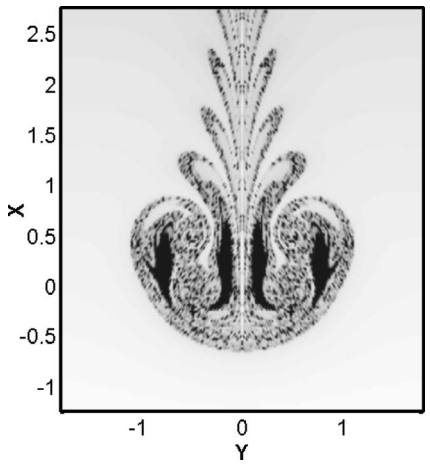

FIG. 11. A typical plot of residence times in the vicinity of the vortical structures. Darker portions indicate longer residence times. Fluid in the immediate neighborhood of each blob moves forever with it. The lobes in the upper region consist of fluid which is drawn into the vicinity, and spends a long time there.

entrainment is a nonmonotonic function of buoyancy, and will attain a maximum at some critical buoyancy. Figures 6–8 depict the manifolds at different U_b. Here U_b is nondimensionalized with the average streamwise velocity of the vortices (U_s) in the absence of buoyancy. The change in the manifold structure illustrates the effect of buoyancy on entrainment. The fluid contained within a lobe formed by the intersection of the stable and unstable manifolds is entrained in one time period of the basic motion. The entrainment is thus given by the area of a lobe. It has been checked that the area within each lobe is identical. Figure 9 depicts the entrainment rate at various pair spacings Δx, where Δx is the maximum streamwise distance during the leap-frog cycle. One finds a maximum for every given initial pair spacing, which is independent of the spacing.

The primary difference between leap-frogging vortex rings (LFVR) and LFVP is that in the LFVR, the self-induced velocity can be independently controlled by adjust-

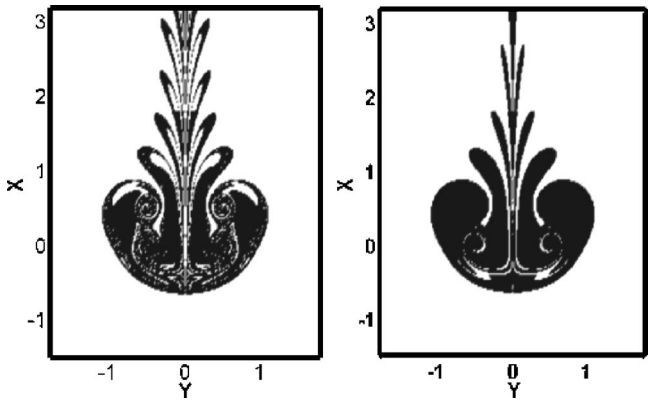

FIG. 12. Effect of viscosity on entrainment. The viscosity is 10^{-5} in nondimensional units for the left-hand panel, while for the right-hand panel it is 10^{-3}. The initial separations of the vortices for both simulations are $\Delta Y=1$ and $\Delta X=0.5$. The simulations are both run up to time=80.

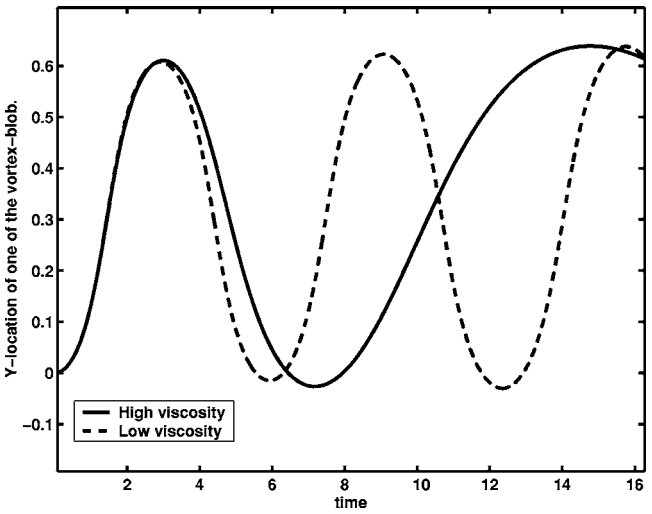

FIG. 13. The time period of leap-frog in a low viscosity simulation is nondimensional time units for the initial configuration considered (dashed line). The period is maintained over several oscillations. However, for the same initial configuration, when the viscosity is high (solid line), the leap-frogging behavior is similar at short times, but slows down significantly at later stages.

ing the ring thickness, so fixed points can vanish even without buoyancy.

The discussion so far has been restricted to inviscid flow. The viscous problem is treated in the following section, by a two-dimensional vortex-method based simulation.

V. EFFECT OF VISCOSITY

The system of two leap-frogging vortex pairs is simulated here in two dimensions by a vortex method. Two pairs of vortex blobs, of initial configuration as shown in Fig. 10 are located in an ambient medium consisting of tracer particles, as shown. The coordinate system and the computational domain move forward with the average velocity of the vortices. During each time period, tracer particles in the flow as well as the blobs of vorticity propagate in accordance with the Biot-Savart law. Viscosity is accounted for in the diffusion of the vortex core alone [14], and the effect on a given blob of self-advection due to diffusion is neglected. We are interested in monitoring the residence times of various portions of flow, where the residence time of a location is characterized by the time that a particle originating there spends within the computational domain. As discussed in Ref. [8], particles within the stable manifold display large residence times, and the tangles obtained in residence time plots are thus a measure of entrainment in the system. In other portions of the domain, trajectories are deviated by the presence of the vortices, but the fluid is not entrapped. Tracer particles in such regions leave the domain of interest within a short time. A typical residence-time plot is shown in Fig. 11, where darker portions indicate longer residence times.

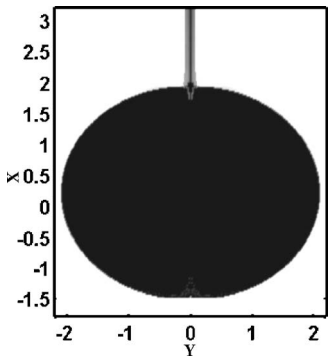

FIG. 14. Effect of initial spacing of vortex pairs in the presence of viscosity. The viscosity is 10^{-3}, and the initial separations of the vortices are $\Delta Y=2$ and $\Delta X=0.4$. As in the inviscid case (not shown) the entrainment is shut off at low pair separations.

In Fig. 12 the effect of increasing the viscosity by a factor of 100 on the entrainment region is shown. It is immediately apparent that the number of lobes reduce with increasing viscosity, but the residence time within a lobe is higher. The area of each lobe has been measured to be about the same, for both levels of viscosity. In other words, the amount of fluid entrained during one leap-frog cycle is about the same, but the higher residence time could mean greater opportunity for mixing at a molecular level between the original and entrained fluid. However there is a significant reduction in the entrainment *rate*. This is because as time progresses, diffusion smears out the vortex core, which results in a reduction in the induced velocities and a slowing down of the leap-frogging process, as shown in Fig. 13.

The effect of separation between the two pairs of counterrotating vortices for the viscous case is similar to what is seen in the invisicd case, an example is shown in Fig. 14.

VI. SUMMARY

To summarize, the present paper carries the proof of nonintegrability of two-dimensional leap-frogging vortex pairs using the Melnikov technique. The tangling of the manifolds of the hyperbolic fixed points gives rise to chaos for any finite separation between the two corotating pairs. This in turn gives rise to entrainment, which varies nonmonotonically with the relative speeds of the vortical and nonvortical portions of the flow. Viscosity slows down the dynamics significantly and thus reduces entrainment rate.

ACKNOWLEDGMENTS

The authors would like to acknowledge M. Tyagi for having useful discussions while doing this work. Funding from the DRDO, Government of India, is gratefully acknowledged. One of the authors (S.M.) would also like to thank Jawaharlal Nehru Centre for Advanced Scientific Research for supporting this work by their Summer Research Fellowship Program.

[1] R. Govindarajan, Phys. Rev. Lett. **88**, 134503 (2002).
[2] R. Narasimha and L. Venkatakrishnan, Proceedings of the Eighth Asian Congress on Fluid Mechanics, 1999, p. 275.
[3] H. Aref, Phys. Fluids **14**, 1315 (2002).
[4] A. Pentek, T. Tel, and Z. Toroczkai, J. Phys. A **28**, 2191 (1995).
[5] J. C. McWilliams, J. Fluid Mech. **146**, 21 (1984).
[6] A. J. Basu and R. Narasimha, J. Fluid Mech. **385**, 199 (1999).
[7] G. S. Bhat and R. Narasimha, J. Fluid Mech. **325**, 303 (1996).
[8] V. Rom-Kedar, A. Leonard, and S. Wiggins, J. Fluid Mech. **214**, 347 (1990).
[9] A. A. Bagrets and D. A. Bagrets, Chaos **7**, 368 (1997).
[10] A. H. Nayfeh, *Perturbation Methods* (Wiley, Interscience, New York, 2000).
[11] R. Govindarajan, A. Leonard, and S. Wiggins, in *Lecture Notes in Physics*, edited by C.-H. Bruneau (Springer, New York 1998), pp. 482–487.
[12] S. Wiggins, *Chaotic Transport in Dynamical Systems* (Springer, Berlin, 1992).
[13] J. Guckenheimer and P. Holmes, *Nonlinear Oscillations, Dynamic Systems, and Bifurcations of Vector Fields* (Springer-Verlag, New York, 1983).
[14] A. Leonard, J. Comput. Phys. **37**, 289 (1980).